AE-507

UDC 537.531:
535.42:
539.2.016

AE-507

X-Ray Characterization of Non-Equilibrium Solid Solutions

A. Brown and Ö. Rosdahl

AKTIEBOLAGET ATOMENERGI

STUDSVIK, NYKÖPING, SWEDEN 1975

X-RAY CHARACTERIZATION OF NON-EQUILIBRIUM SOLID SOLUTIONS

Allan Brown and Östen Rosdahl

AB Atomenergi, Studsvik, S-611 01 Nyköping, Sweden

ABSTRACT

The Rudman approach to composition line broadening in X-ray diffraction patterns, originally designed for the study of diffusion in alloys, is seen to provide a basis for characterizing inhomogeneous solid solutions. Limitations, imposed on this treatment when the cell dimensions of the primary components differ by less than 0.1 Å, are attributable to experimental effects such as instrument broadening. These limitations can be overcome by a rigorous numerical treatment of the measured data. Thus, separate elimination of the $K\alpha_2$ radiation component followed by iterative deconvolution are advocated for the recovery of the intrinsic broadening. This course of action is made possible chiefly through the availability of large, fast memory computers and primary data recorded in the form of a step scan on punched paper tape.

The characteristics of inhomogeneous solid solutions made available by the above treatment are the identity of closely similar, solid solution phases, the frequency distribution curve for a chosen component, and the degree of homogeneity of the X-ray sample.

LIST OF CONTENTS

1. INTRODUCTION

The analysis of solid solutions by X-ray diffraction depends upon the fact that, with only few exceptions, the solute and solvent exhibit different values of unit cell dimension. Solid solution phases are therefore characterized by cell dimensions that are intermediate between those of the primary components. In many systems, the cell dimension is linearly proportional to the atomic or molecular fraction of the species in solution; in other systems, the relationship is described by a more or less regular curve. In either case, evaluation of the unit cell dimension from measurements of the diffraction pattern permits the solute content in the X-ray specimen to be determined.

The above, simple approach to solid solution characterization requires the fulfillment of two essential conditions if it is to provide unambiguous answers. Thus, the difference between the values of the cell dimension for the primary components, combined with the resolution of the recording instrument, should be such as to allow clear separation of solid solution phases differing by at most 5 at % or mol%. In addition, the X-ray specimen should be chemically homogeneous so that sharp, well-defined diffraction patterns are available for measurement; subsequent evaluation of composition can then be made with a maximum error of ± 5 %.

If the prescribed conditions are not met with, analysis is complicated by broadening of the diffraction lines to a point where measurement can only indicate the range of compositions present in the sample. In the present context, such line broadening can be considered to have two origins, namely short-range chemical inhomogeneities, and the broadening produced by instrumental aberrations

and the composition of the X-ray spectrum, if this is not strictly monochromatic. Thus a solid solution that has not attained equilibrium will contain a range of compositions, each of which is associated with a distinct value of the unit cell dimension. In making their separate contributions to the overall diffraction pattern these components phases provide closely spaced groups of reflections that overlap to yield broadened diffraction profiles. Description of this composition broadening is clearly desirable in order to permit characterization of the solid solution sample and specification of the degree of homogeneity attained. Such characterization acquires special significance when it is remembered that many solid solutions attain full equilibrium only very slowly but may nevertheless serve their purpose once a given level of homogeneity has been exceeded.

In the meantime satisfactory measurement is hindered by instrument broadening and, where monochromatic X-rays are not used, by the overlap of the spectral components such as the $K\alpha_1$ and $K\alpha_2$ components normally encountered in routine diffractometry. As long ago as 1960, however, Rudman (1) indicated a partial solution to this problem. Thus, he proposed that study be restricted to profiles in the angular region beyond 90° (2θ) where the instrument broadening changes only slowly with angle. Under such conditions, treatment of the profile to remove the $K\alpha_2$ contribution served to uncover broadening in 50 % solutions whose primary components had cell dimensions differing by more than 0.1 Å. With instrument broadening such that the full width at half maximum height (FWHM) is 0.2° (2θ), for an ideally sharp peak at 120° (2θ), it was shown that compositional changes as small as 1 % could be detected by this method.

The removal of instrument broadening using the Stokes' (2) method for deconvoluting diffraction profiles was not found to be advantageous. This could be attributed to oscillations produced in the tails of the diffraction profiles by the Fourier treatment on which Stokes' method is based. Such oscillations are very easily induced by the presence of statistical errors in the measured data or even by an incorrect subtraction of the background continuum.

While recognizing the essential truth of Rudman's argument, it is important to realize that many technically valuable solid solutions are based on primary components whose cell dimensions differ by less than 0.1 Å. In many instances, therefore, characterization of an inhomogeneous sample is rendered difficult by the appreciable instrument broadening which, despite the elimination of the $K\alpha_2$ component, smears out the intensity distribution of closely spaced peaks into a single, irregular profile. Deconvolution of the observed profile therefore becomes a worthwhile proposition, particularly in view of the fact that instrument broadening may reduce the resolution expected for the slit system in use, by a factor of up to three. Moreover, the period since 1960 has seen the development of large core-memory computers with high operational speeds. The opportunity accordingly exists for applying more effective, if numerically more laborious, methods of deconvolution then that described by Stokes.

The following account represents a more rigorous treatment of the Rudman approach to composition broadened profiles, facilitated by a code written in Fortran IV for a CDC Cyber 73 computer. This

numerical treatment of recorded profiles was first employed on the results of diffusion experiments with UO_2 and oxides such as CeO_2 and Gd_2O_3. Since then it has been found to provide a means of describing the level of homogeneity in UO_{2+x} powders used for fuel pellet manufacture. Application to inhomogeneous solid solutions would appear to be quite general provided that certain basic information about the system is available.

2. CORRECTION FOR SPECTRAL AND INSTRUMENT BROADENING

2.1. Elimination of the $K\alpha_2$ component

Recovery of the diffraction profile containing only information about compositional variations in the form of intrinsic broadening is accomplished in two steps. Following the approach proposed by Rudman, the contribution to the profile from the $K\alpha_2$ component of the X-ray spectrum is removed using Keating's (3) method. The starting point for this treatment is a step scan of a diffraction profile given by the solid solution. This is recorded in the angular range beyond 110° (2θ) between limits determined by the diffraction angles for corresponding peaks from the primary components. These limits are chosen with respect to the level of background intensity so that both solid-solution and unreacted-component peaks are encompassed by the scan. In our case, the scan is made with large step lengths and maximum counting times (0.1° (2θ) and 100 secs) over the background, changing to shorter steps and counting times (0.01° (2θ) and t for 10 000 counts)

on passing over intensity maxima. This strategy, however, is only a detail aimed at improving the efficiency of the measuring process and does not materially alter the validity of the results, except in so far as it affects the statistical reliability of the measurements.

The step scan is conveniently recorded on punched tape as a set of values of counts per second, I_t and diffraction angle 2θ. Subsequent computer treatment of this data first provides a new set of I_t values at a uniformly spaced set of 2θ values, using, for example, parabolic interpolation. Background is then subtracted between angles, at or near the scan limits, defined by the presence of intensity minima.

According to Keating, identity of moment distribution for the $K\alpha_1$ and $K\alpha_2$ spectral components yields

$$h(\kappa) = f(\kappa) + \frac{1}{R} f(\kappa')$$

for the relationship between the observed profile $h(\kappa)$ and the profile after α_2 elimination $f(\kappa)$. Here, $\kappa = (4\pi/\lambda_1)\sin\theta$, $\kappa' = (4\pi/\lambda_2)\sin\theta$ and $R = I\alpha_1/I\alpha_2$. The α_1-free profile is then obtained by summing a set of n profiles each of which is derived from its predecessor by generally reducing the intensity by the factor R, inverting, and translating along the 2θ axis by an amount given by the difference between $\lambda\alpha_1$ and $\lambda\alpha_2$. The principle of the treatment becomes clear from Fig 1a which shows the original profile $h(\kappa)$ in relation to the first two of the derived series of profiles. Fig 1b shows the results obtained on adding these three data sets. In practice we sum a set of n = 10 profiles to achieve minimal disturbance of the background due to the

addition of the α_2 of the last profile.

The high quality of the result obtained with the Keating treatment is seen in Fig 2 which shows the α_2-free 620 reflection from well-crystallized ThO_2. Calculations made on this profile show that the peak position and centroid differ by less than 0.05° (2θ) signifying a virtually error-free result.

2.2. Recovery of the intrinsic profile

Since the ThO_2 profile, above, has no intrinsic broadening due either to chemical inhomogeneities, microstrain distributions or crystallite sizes less than 0.3 μm, it serves as a measure of the broadening produced by the combined instrumental aberrations. These are effects common to all optical systems that feature divergent beams, imperfect focusing conditions and beam-limiting slit systems.

For a profile with intrinsic broadening, the observed profile h(x) is described as the convolute of the intrinsically broadened profile f(x) with the instrument function g(x) such that

$$h(x) = \int_{-\infty}^{\infty} f(y) \cdot g(x-y)\, dy \qquad (1)$$

Here, f(y)dy is an element of intrinsic broadening, spread out by the broadening function, such that at a position x on the observed distribution, it contributes an intensity

$$f(y)\, dy \cdot g(x-y)$$

The integral equation for h(x) above can be treated iteratively to recover the intrinsic profile f(x). Thus we define

$$f_o(x) = h(x) \tag{2}$$

$$u_n(x) = h(x) - \int_{-\infty}^{\infty} f_n(y) \cdot g(x-y)\, dy \tag{3}$$

$$f_{n+1}(x) = f_n(x) + u_n(x) \tag{4}$$

For a start made in accordance with (1) iteration is performed in accordance with (3) and (4) until $u_n(x)$ is sufficiently close to the statistical level of error expected from the overall number of counts collected during the step scan. In order that the iterative treatment should go to convergence, it is preferable for the instrument function g(x) to be smoothly changing and as nearly symmetrical as possible. This is evidently the case for the $K\alpha_1$ profile of ThO_2 mentioned above. Thus, although it is possible to accomplish the α_2 elimination as an integral part of deconvolution, the instrument function will, in that case, comprise a $K\alpha_1$ and a $K\alpha_2$ component. The resulting increase in the complexity of the instrument function can easily give rise to numerical difficulties. It is accordingly preferable to remove the α_2 component beforehand, particularly as the Keating method seems so very effective.

The great underlying difficulty of deconvolution, using either Fourier methods according to Stokes, or the iterative approach described here, is the association of the measured intensities with statistical errors. These operate so as to produce sharp oscillations in the exact solution of equation 1. The single pass deconvolution according to Stokes lacks the ability to control these oscillations and it becomes difficult to distinguish in the resulting profiles between peaks due to

closely related solid solution components and those originating in statistical intensity errors. The iterative method applied here allows, however, an inspection of the result after each cycle. By applying the condition $f_n(x) \geq 0$ for all x, together with a suitable smoothing of the intermediate result, only major excursions of the intensity curve are allowed to generate peaks in the deconvoluted profile.

The course of iterative deconvolution is illustrated in Fig 3a which shows the curve for the first guess $f_o(x)$ in relation to the curve generated after the first iteration $f_1(x)$, while $u_o(x)$ is the residue after this operation. A test of the effectiveness of this procedure is shown in Fig 3b which concerns the recovery of a simple, idealized profile in the shape of a triangle. This was first convoluted with a Gaussian function to give the smeared profile h(x). Iterative deconvolution was then performed for 20 cycles to give the distribution $f_{20}(x)$ which is a close approximation to the original triangle.

Finally, the deconvolution of two real solid solutions is exemplified in Figs 4 and 5. The first of these refers to a UO_{2+x} powder for fuel fabrication which was known to exhibit a range of chemical composition. The outer profile, obtained before the removal of the $K\alpha_2$ component, merely shows extensive broadening. The inner profile, produced by deconvolution, is rich in detail that indicates the coexistence of small amounts of near stoichiometric UO_2 with more significant amounts of $UO_{2.02}$ and $UO_{2.04}$. The powder is seen to contain aggregates of even more hyperstoichiometric oxides such as $UO_{2.122}$ and $UO_{2.177}$ while the average composition, $UO_{2.029}$, is the value obtained from measurements made on a powder pattern recorded in a Guinier-type focusing camera.

The second example, illustrated in Fig 5, is the result of a diffusion experiment in a powder compact with the composition UO_2-20 CeO_2, after 32 hours at 1700°C. The deconvoluted profile shows that unreacted UO_2 is still present in detectable amounts while the principal solid solution components are a uranium-rich phase, $U_{0.84}Ce_{0.16}O_2$, and $U_{0.78}C_{0.22}O_2$ which lies on the cerium-rich side of the average composition.

The FWHM value for these two phases is roughly 0.08° as compared with the value of 0.21 (2θ) for the uncorrected $K\alpha_1$ profile of ThO_2. In this instance, therefore, the resolution, and thus the ability to detect closely similar solid solution phases, is more than doubled by the deconvolution treatment. With a 1/4° receiving slit, in conjunction with the curved graphite monochromator and a slit-to-specimen distance of 17.6 cm employed in the recording diffractometer, the expected FWHM should be 0.06° (2θ) for well crystallized solid solution components. The resolution actually realized is accordingly close to the maximum attainable with this slit system.

3. CALCULATION OF FREQUENCY DISTRIBUTION AND HOMOGENEITY FROM DECONVOLUTED PROFILES

3.1. Frequency distribution curves

In the preceeding section it was shown that the deconvolution of composition broadened profiles is capable of revealing detail regarding the component phases in the inhomogeneous sample. In the instances quoted, hitherto undetected UO_2 was revealed to be present, in addition to which the compositions of the major phases could be easily identified. Additional, more quantitative descriptions of the

solid solution are needed, however, and can be provided by a plot of the frequency distribution of the solute (oxygen or CeO_2 in the two examples quoted). Again, the treatment follows, in the main, that outlined by Rudman (1). Accordingly, this section will be restricted to a summary of the Rudman approach and to more detailed comments at points where innovations have been made that lead to significant improvements in the results.

An essential requirement is that the relationship between changes of cell dimension and composition has previously been established. Replacing the cell dimension by the d spacing corresponding to a particular hkℓ reflection, this may be expressed as $\delta d/\delta c$ where c represents composition. The minimum detectable composition interval is then given by

$$\Delta c = \Delta d/(\delta d/\delta c)$$

where Δd is the interplanar spacing resolution for the selected profile. Differentiation of Bragg's law and substitution for Δd then yields

$$\Delta c = \cot\theta \Delta\theta/(1/d)(\delta d/\delta c)$$

For the UO_2-CeO_2 system, $\delta d/\delta c$ follows Vegard's law and the 620 reflection occurs between the limits 125.87 and 128.37° (2θ) for UO_2 and CeO_2 respectively using $CuK\alpha_1$ radiation. Accordingly, $\cot\theta \simeq 0.5$ and $1/d(\delta d/\delta c) = 1.07$, while $\Delta\theta \simeq 0.35°$ (or 0.006 radians) from the minimum FWHM value for a deconvoluted profile. Substitution of these values in the equation for Δc yields a composition resolution of 2.8 % CeO_2. The diffraction interval between the above-mentioned angular limits can thus be inspected at 37 intervals corresponding to uniform steps of 1/d and the intensity recorded at each point treated to obtain the relative number of molecules N(c) of composition c.

Following Rudman, the expression used to correct the observed intensity given by a simple f. c. c. solid solution is given as

$$N(c) \propto \frac{[\, d'(c)/d(c)] \tan\theta}{[\, cf_B + (1-c) f_A]} \cdot \frac{\sin^2\theta \cos\theta}{1 + \cos^2 2\theta} \cdot g(\theta)$$

where

$g(\theta)$ represents the observed profile expressed as a variation of intensity with angle

f_A and f_B are the scattering powers of the atomic species involved in solid solution formation

$\frac{\sin^2\theta \cos\theta}{1 + \cos^2 2\theta}$ is the reciprocal of the Lorenz-polarization factor for a powder intensity registered at angle 2θ

$\frac{d'(c) \tan\theta}{dc}$ represents the change of diffraction interval with composition $\delta d/\delta c$

The above expression may then be reduced to

$$N(c) = Q_\theta \cdot g(\theta)$$

where Q_θ is the combined correction factor. The procedure for obtaining N(c) from the measured intensities is readily understood with reference to Fig 6. Intensity I′, measured at diffraction angle $2\theta'$, corresponds to a solid solution of composition c′. The diagram shows that the value of the correction factor corresponding to this composition is Q′. Successive treatment of the diffraction profile in Fig 5 between $2\theta_{UO_2}$ and $2\theta_{CeO_2}$ yields the frequency distribution curve for cerium dioxide in the solid solution formed after 32 hours heating at 1700°C, as shown in Fig 7.

It is important to note that in the above diagram, correction is made for the spread of the diffraction profile of unreacted UO_2. With an ideal optical system, this intensity would be collected in a delta function at the 2θ value for UO_2. If the spread observed in Fig 5 is ignored the resultant value of N(o) will be too low since intensity at $2\theta < 125.87^o$ is neglected while that at $2\theta > 125.87^o$ is treated as though it contained contributions from Ce atoms. A more consistent approach is therefore obtained by accumulating the intensity distributed symmetrically about 125.87^o, up to a limit given by the low angle tail of the UO_2 peak, and placing it at the peak position. This is then treated as a single intensity to yield a more representative value of N(o).

The frequency distribution curve possesses the important property that the average composition of the solid solution is given by

$$\bar{c} = \int_o^1 cN(c)dc / \int_o^1 N(c)\,dc$$

Thus if $\bar{c}$, evaluated from the curve, differs from that of the sample as a whole, as obtained by chemical analysis for example, the treatment thus far is subject to error. Likely sources of experimental error include the possibility that the composition of the X-ray specimen departs from that of the sample due to gross chemical inhomogeneities. Alternatively, the subtraction of the X-ray background may have been made incorrectly, leading to a general raising or lowering of N(c) for all c. Thus in tests made on the profile of the above-mentioned UO_2 - 20 CeO_2 solid solution, the background was reduced by 1000, a level that corresponds to 0.7 % of the intensity maximum of

the solid solution peak. This change led to a decrease in $\bar{c}$ by 0.008. Similarly, the angular calibration of the recording diffractometer may be in error. The intensity distribution in the measured interval will accordingly be displaced along the 2θ axis with respect to limits assigned for the primary components of the solid solution. Tests show that for the UO_2 - 20 CeO_2 profile, a general increase in 2θ by 0.02° above the true value leads to an increase in $\bar{c}$ by only 0.011 while a change of 0.07° produces an increase in $\bar{c}$ by as much as 0.05.

The significance of corrections of the above type, performed on the experimental data, can be more readily appreciated if it is remembered that $\bar{c}$ is the first moment of the frequency distribution. The greatest influence will therefore be experienced from corrections leading to changes in N(c) at values of c differing greatly from that of $\bar{c}$ itself.

In mixed oxide systems there is also the possibility that the O/M ratio, assumed thus far to have a specific value, might have been disturbed as a result of oxidation or reduction with a consequent displacement of the solid solution profile. This situation is equivalent to an erroneous assignment of limiting angles for one or both of the primary components in the recorded profile. If other sources of experimental error can be excluded it therefore becomes possible to investigate possible changes in O/M by adjusting these limiting angles until the calculated $\bar{c}$ agrees with the known ratio of the two metal components in the sample. Thus in the example quoted here partial reduction of CeO_2, leading to the presence of Ce_2O_3 in the solid solution, would lead to values of $\bar{c} < 0.2$. The upper limiting angle should then be decreased in small steps until the condition

$\bar{c} = 0.2$ is fulfilled. The displacement required to satisfy this condition can then be used to determine the change in O/M from the known diffraction angle for CeO_2 and that extrapolated for cubic Ce_2O_3.

3.2. Effective penetration curves and homogeneity

The second important property of the frequency distribution curve is that it serves as a basis for calculating the effective penetration achieved by interdiffusion of the primary solid solution components. This quantity is defined as

$$y = \int_0^c N(c)\, dc \Big/ \int_0^1 N(c)\, dc$$

and is plotted in a normalized diagram as a function of c so that $0 \leq y \leq 1$ and $0 \leq c < 1$. In Fig 7, the penetration diagram of y versus c is shown in relation to the frequency distribution curve from which it has been derived. It is noteworthy that in the range $0 < c < 0.1$, the value of the cumulative integral y is almost constant and non-zero. This result is produced by the relatively large value of N(o) which corresponds to the amount of unconsumed UO_2 in the X-ray sample. It accordingly represents a situation in which the UO_2 particles have not yet been completely penetrated by CeO_2.

The value of y rises sharply in the range $0.1 < c < 0.3$ where the body of the solid solution is located. It is evident that the shape of the curve will be determined by the width of the frequency distribution in this compositional range. It follows that for a fully homogeneous sample which gives an ideally narrow diffraction peak, the value for y should rise instantaneously from zero to unity at the value of $\bar{c}$, in this instance 0.2.

Finally in Fig 7, the value of y is seen to rise only slowly in the range $c > 0.4$. This corresponds to the fact that diffracted intensity from unreacted CeO_2 and cerium-rich solid solutions is indistinguishable from the background scattering, which happens to be relatively heavy in the angular range concerned. The absence of CeO_2 and cerium-rich phases from the sample is therefore reflected by the way in which the plot of y terminates at a value of c close to 0.5.

In Fig 8, the plot of y versus c has been redrawn following further background subtraction to correct for possible diffuse scattering. The diagram is seen, in this form, to resemble the penetration diagrams obtained in one-dimensional diffusion studies where c is plotted as a function of x, measured in some convenient unit of length. In true penetration diagrams, however, the occurrence of assymetrical diffusion across the geometrical boundary between the two components means that the position of this boundary along the x axis has no significance when the underlying diffusion phenomena are studied. It accordingly becomes necessary to find the position of the Matano interface (4, 5). This separates the region along the x-axis occupied by the number of interdiffused atoms of one species from the corresponding region containing the identical deficit of this species.

X-ray penetration diagrams differ radically from true penetration diagrams in that they are insensitive to the geometrical nature of the interdiffusing system and therefore behave as if they were all symmetrical. From

$$\bar{c} = \int_0^1 cN(c)\,dc \Big/ \int_0^1 N(c)\,dc$$

integration by parts yields

$$\bar{c} = 1 - \int_0^1 \left[\int_0^c N(c)dc\right] / \int_0^1 N(c)\,dc$$

= area under curve of c versus y which is accordingly constant at all stages of diffusion. The boundary, y′, to which the degree of penetration is referred, is given by the condition $\int_0^1 (y-y')dc = 0$. This merely states that the number of atoms penetrating below the boundary at y′ is equal to the number vacating the region beyond y′. With reference to Fig 8, area α equals area β. Since the X-ray penetration diagram has unit dimensions, and $\bar{c} = \alpha + \gamma$ in Fig 8 it is readily seen that these two requirements lead to a value of $y' = 1-\bar{c}$ at all stages of diffusion.

It should be observed that this formulation departs from that given by Fisher and Rudman (6) and many subsequent investigators (see 7 for example). These authors base their treatment of X-ray penetration curves on the computed position of a Matano interface. It should be stressed, however, that the value of y′ differs from $1-\bar{c}$ if, and only if, the value of $\bar{c}$ derived from the frequency distribution curve deviates from the average composition of the solid solution.

Fig 8 is, in fact, the effective penetration curve computed for the UO_2-20 CeO_2 solid solution depicted in Figs 5 and 7. The definition of homogeneity follows directly from a consideration of this diagram. Thus the extent to which CeO_2 has diffused into the solid solution after a given treatment is given by the area under the curve at $y \leq 0.8$. It is evident that, for equilibrium conditions under which a completely homogeneous solid solution has been formed, the area occupied would correspond to the rectangle $c = 0.2$, $y = 0.8$. The ratio between these two areas serves as a measure of the degree of homogeneity

attained in the measured solid solution. Expressed generally this becomes

$$H = \frac{\int_{0}^{c_{y=1-\bar{c}}} (1-\bar{c}-y)dc}{\bar{c}(1-\bar{c})}$$

In Fig 8, the value of H is computed to be 87 %.

3.3. Preliminary consideration of errors

Tests have been made to investigate the effect, on the calculated homogeneity, of errors in the treatment of the diffraction profile and frequency distribution curve. In this connection it should be noted that the penetration curve in Fig 8 corresponds to a treatment of the measured data that yields a value of $y' = 0.8$. This is in accordance with the composition of the solid solution which is known to contain a molecular fraction of CeO_2 equal to 0.2.

Earlier in this section it was pointed out that the width of the distribution curve determines the shape of the plot of y versus c. It is therefore evident that instrument broadening, which reduces the height and widens the base of the diffraction profile, will tend to reduce the value of H calculated from the penetration curve. Similarly in section 3.1, background level, error in diffraction angle (profile displacement by $\Delta 2\theta$) and the spread of the peak originating from unconsumed UO_2, were all mentioned as capable of producing errors in $\bar{c}$. The table below, which lists calculated H, y' and the associated error in $\bar{c}$, indicates the extent to which these effects influence the result.

Status of calculation	H (%)	Error in $\bar{c}$	y′
All corrections included	87.5	± 0	0.8
No correction for spread of UO_2	86.7	+ 0.039	0.761
Profile displaced by $+0.02^{o}(2\theta)$	88.9	+ 0.011	0.789
General background of +1 000 (0.7 % of peak maximum)	81.5	+ 0.011	0.789
No deconvolution of profile	69.4	+ 0.104	0.696

It is interesting to note that, in the profile shown in Fig 5 where the amount of residual UO_2 is relatively small, correction for the spread of UO_2 and an angular displacement of + $0.02^{o}(2\theta)$ in the profile have little effect on the calculated homogeneity. On the other hand, raising the background level and, in particular, deconvolution of the profile produce marked changes in H. It will be observed that in each instance, the associated error in $\bar{c}$ leads to a value of y′ which departs by a corresponding amount from the prescribed value of 0.8. In previous publications where effective penetration has been used to calculate H, the assumed existence of a Matano interface has made it possible to accept such erroneous values of y′ with consequences for the evaluation of H that are evident from the above table.

4. CONCLUSIONS

Materials featuring a range of solid solubility are frequently obtained in a non-equilibrium condition that entails short-range chemical inhomogeneity. X-ray diffraction patterns of such materials demonstrate broadened reflections and an unambigous interpretation of such patterns, based on measurements of line position alone, is impossible. Measurement of the intensity distribution within a selec-

ted profile as a function of diffraction angle provides a more useful basis for characterization. After suitable treatment to free these measurements from instrumental effects, the principal phases present in the inhomogeneous sample can be identified. If the relationship between change of cell dimension and composition is known, and the crystal structure of the solid solution has been determined, a frequency distribution plot of N(c) versus c can then be made for a selected component. This curve should include correction for the presence of unreacted components that provide diffraction peaks at the boundaries of the diagram. The value for the average composition $\bar{c}$, calculated from the frequency distribution, should agree with that for the sample as a whole. After correction for experimental errors, residual departures in $\bar{c}$ indicate the presence of gross compositional variations in the sample or, in mixed oxide systems, reduced or oxidized states.

The frequency distribution curve and the deconvoluted profile provide diagrammatic characterization of the X-ray sample. X-ray diffraction serves to accumulate information concerning the nature of the component phases from the separate crystals of which the sample is composed. This information is organized in a form which resembles that obtained from a diffusion couple. Thus the primary constituents occupy positions at the extreme limits of the angular range of interest while intermediate solid solutions are arranged systematically in accordance with composition. Numerical treatment of the frequency distribution curve derived from the profile is then carried through to provide an X-ray effective penetration curve with c and y as axes where

$$y = \int_0^c N(c)\, dc / \int_0^1 N(c)\, dc$$

By analogy with the penetration curve obtained from diffusion sample experiments, the amount of diffused material is seen to be given by the area under the curve between $y = 0$ and the diffusion boundary. In diffusion sample experiments, however, it becomes necessary to determine the position of this boundary in terms of the Matano interface. In X-ray penetration diagrams, the process of normalization, and the absence of physical dimensions make the calculation of a Matano interface irrelevant. The diffusion boundary is accordingly constant at a value of $y = 1 - \bar{c}$.

The ratio between the area of diffused material and the area given by the product $\bar{c}(1 - \bar{c})$, which corresponds to the rectangle obtained for a completely homogeneous material, is a unique value for the homogeneity of the sample.

REFERENCES

1. RUDMAN, P. S.
An X-ray diffraction method for the determination of composition distribution in inhomogeneous binary solid solutions.
Acta Cryst 13 (1960) p. 905.

2. STOKES, A. R.
A numerical Fourier-analysis method for the correction of widths and shapes of lines on X-ray powder photographs.
Proc. Phys. Soc., London, 61 (1948) p. 382.

3. KEATING, D. T.
Elimination of the $\alpha_1\alpha_2$ doublet in X-ray patterns.
Rev. Sci. Instr. 30 (1959) p. 725.

4. MATANO, C.
On the relation between the diffusion - coefficients and concentrations of solid metals.
Japan J. Phys. 8 (1933) p. 109.

5. RHINES, F. N. and MEHL, R. F.
Rates of diffusion in the alpha solid solutions of copper.
Trans. AIME 128 (1938) p. 185.

6. FISHER, B. and RUDMAN, P. S.
X-ray diffraction study of interdiffusion in Cu-Ni powder compacts.
J. Appl. Phys. 32 (1961) p. 1604.

7. HECKEL, R. W.
An analysis of homogenization in powder compacts using the concentric - sphere diffusion model.
Trans. ASM 57 (1964) p. 443.

/Eli

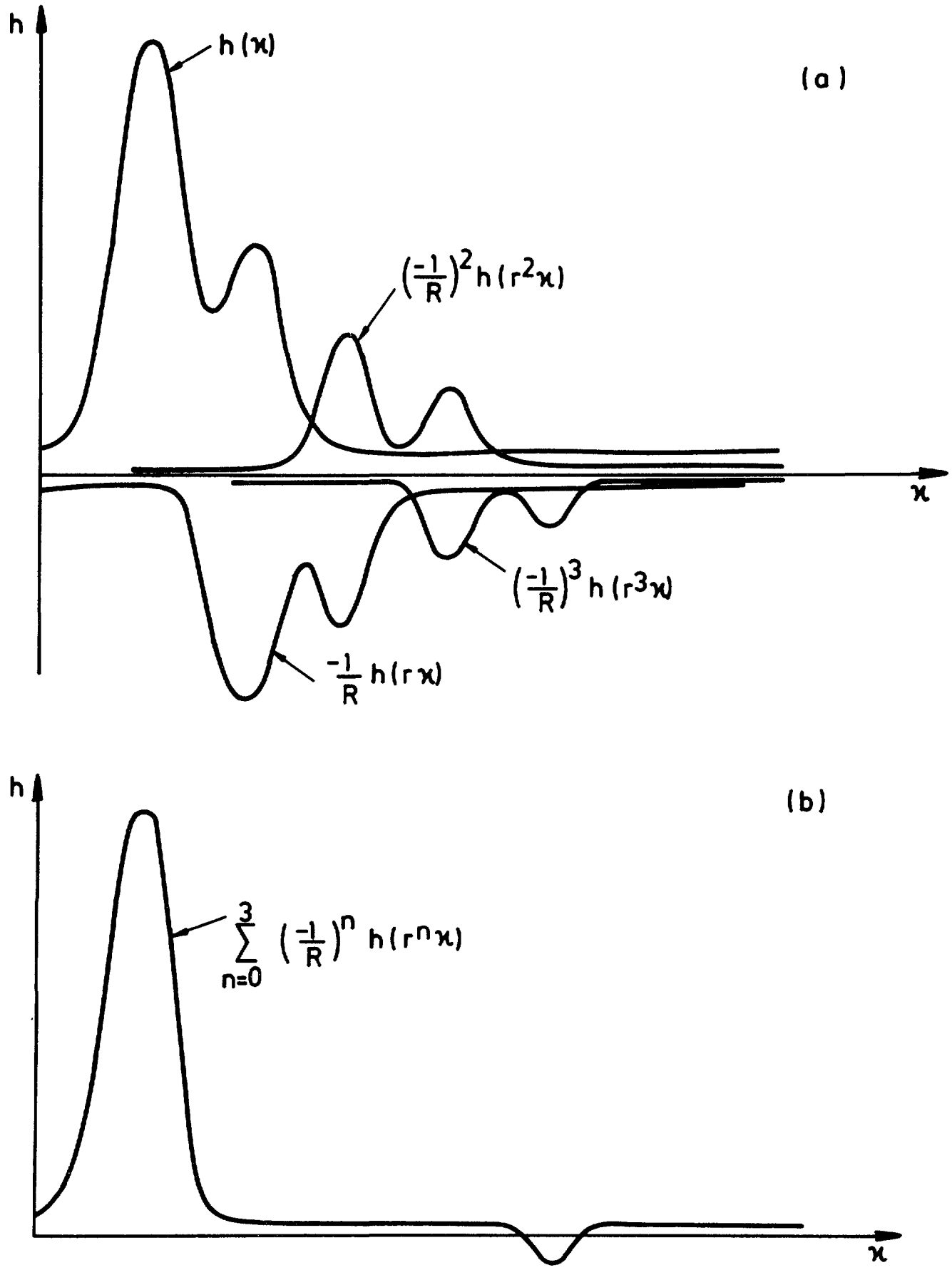

Fig. 1 α_2-Subtraction according to Keating

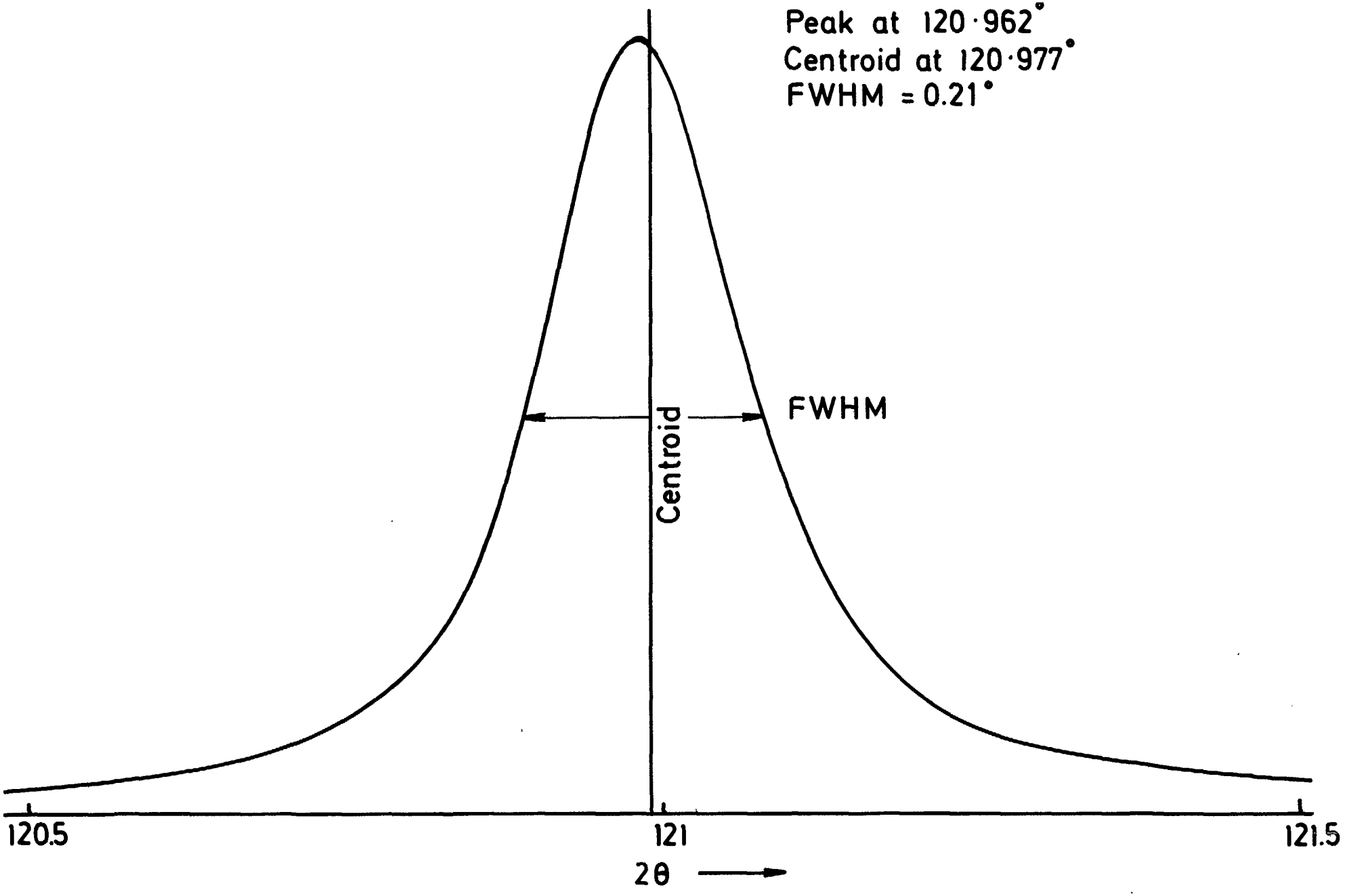

Fig.2 Diffractometer Instrument Function : ThO_2 620

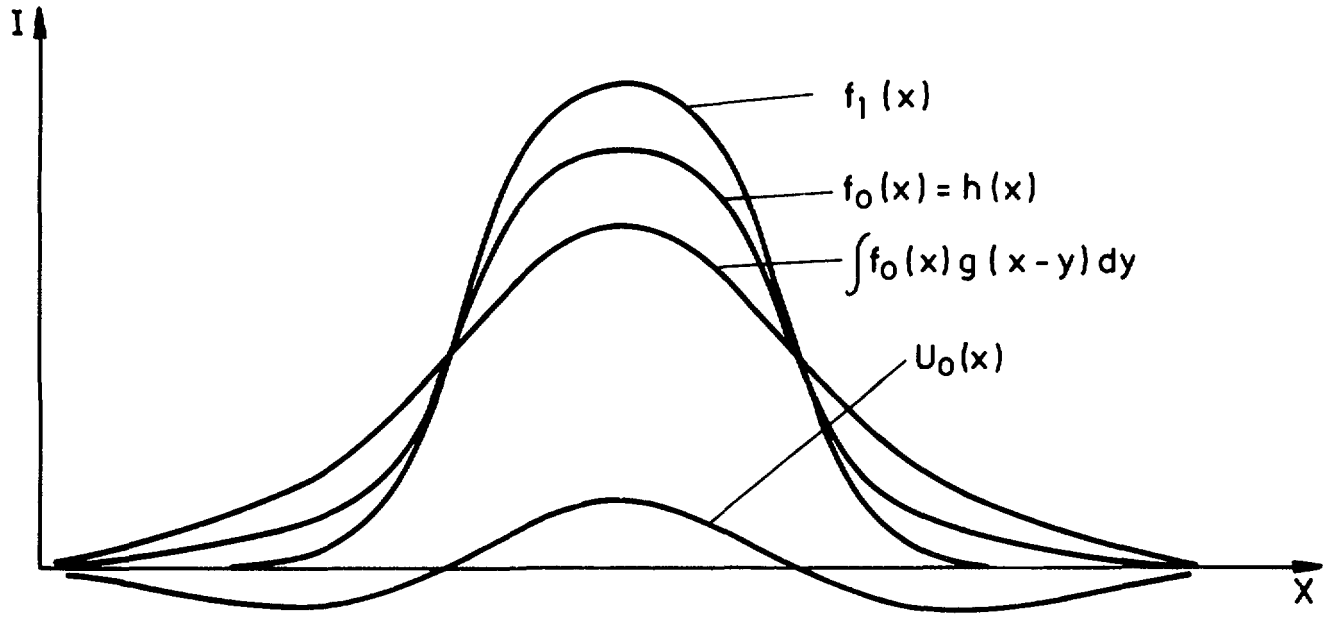

Fig.3a Functions used in iterative deconvolution

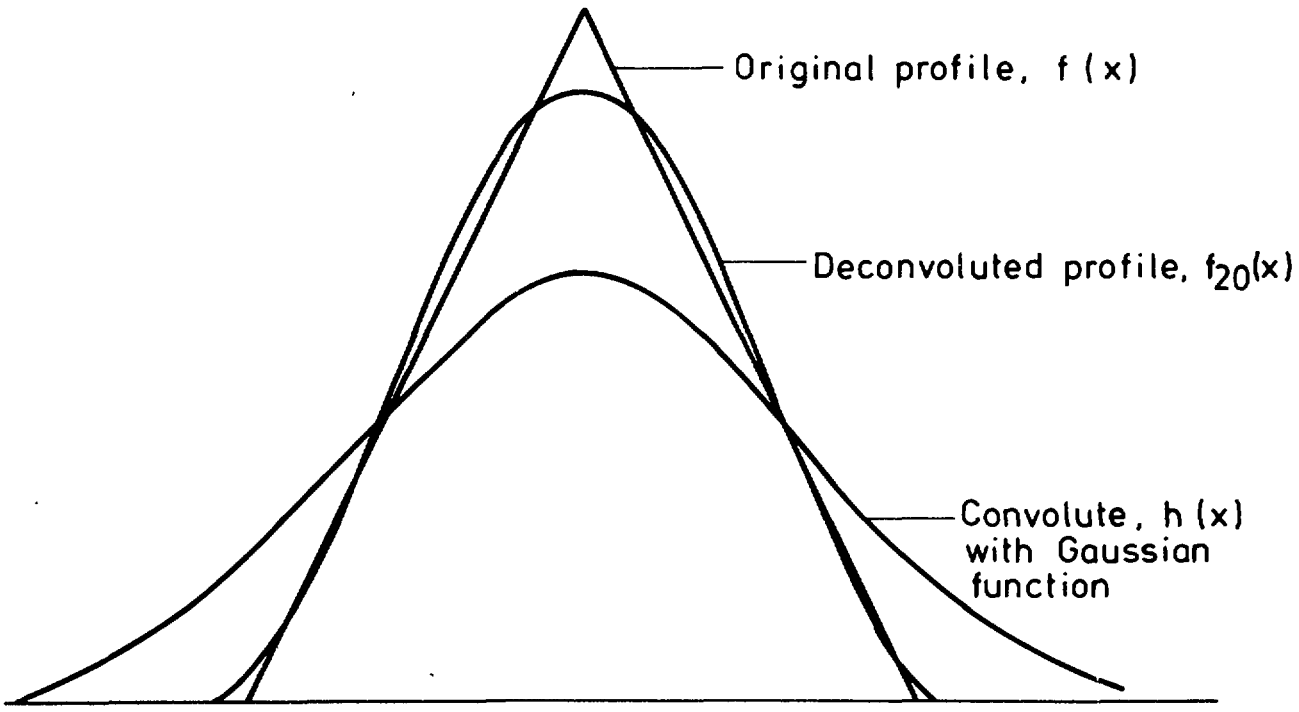

Fig.3b Test of recovery by iterative deconvolution

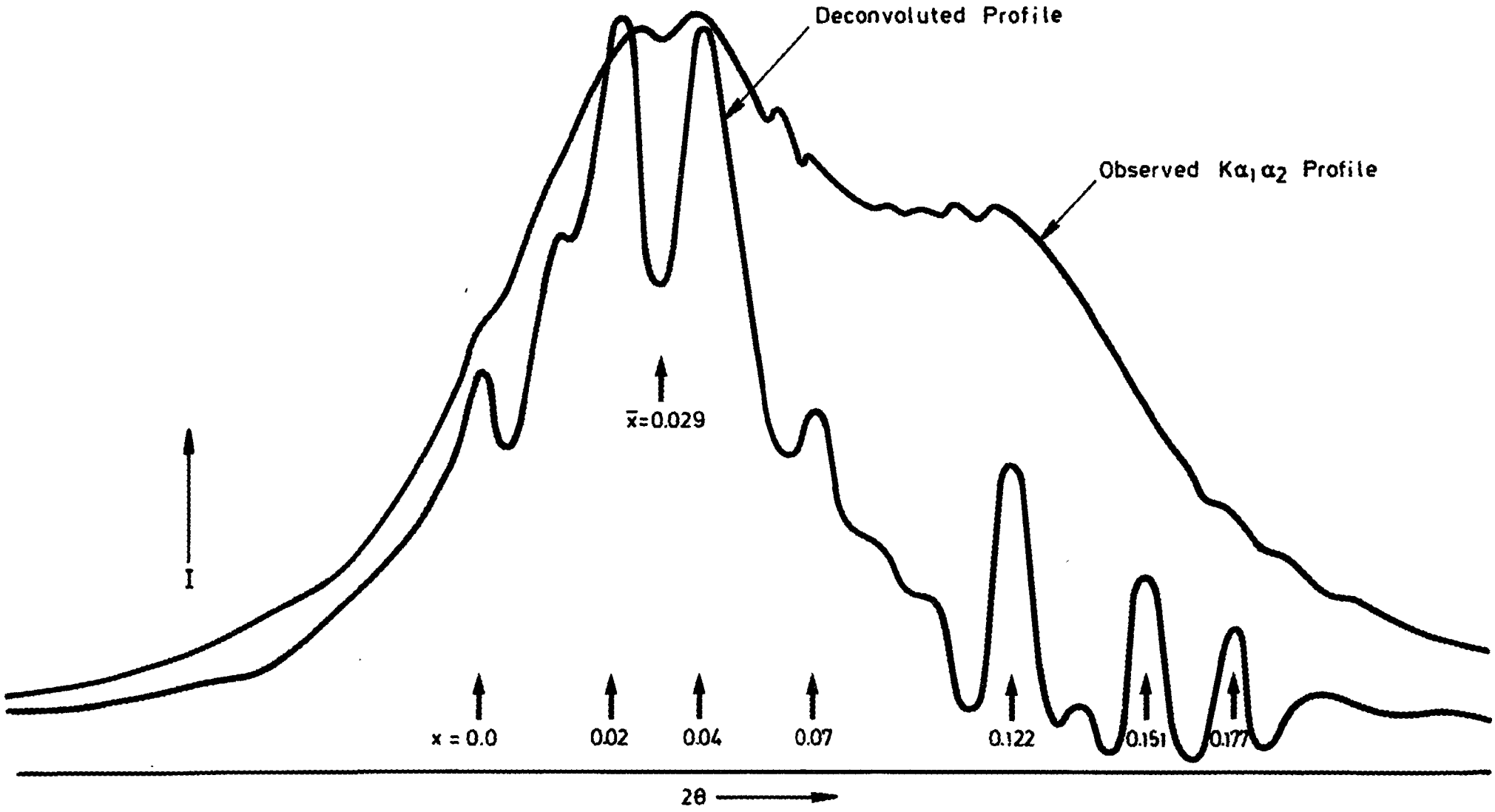

Fig.4 Observed and Deconvoluted 620 Profile of UO_{2+x} : $\bar{x} = 0.029$

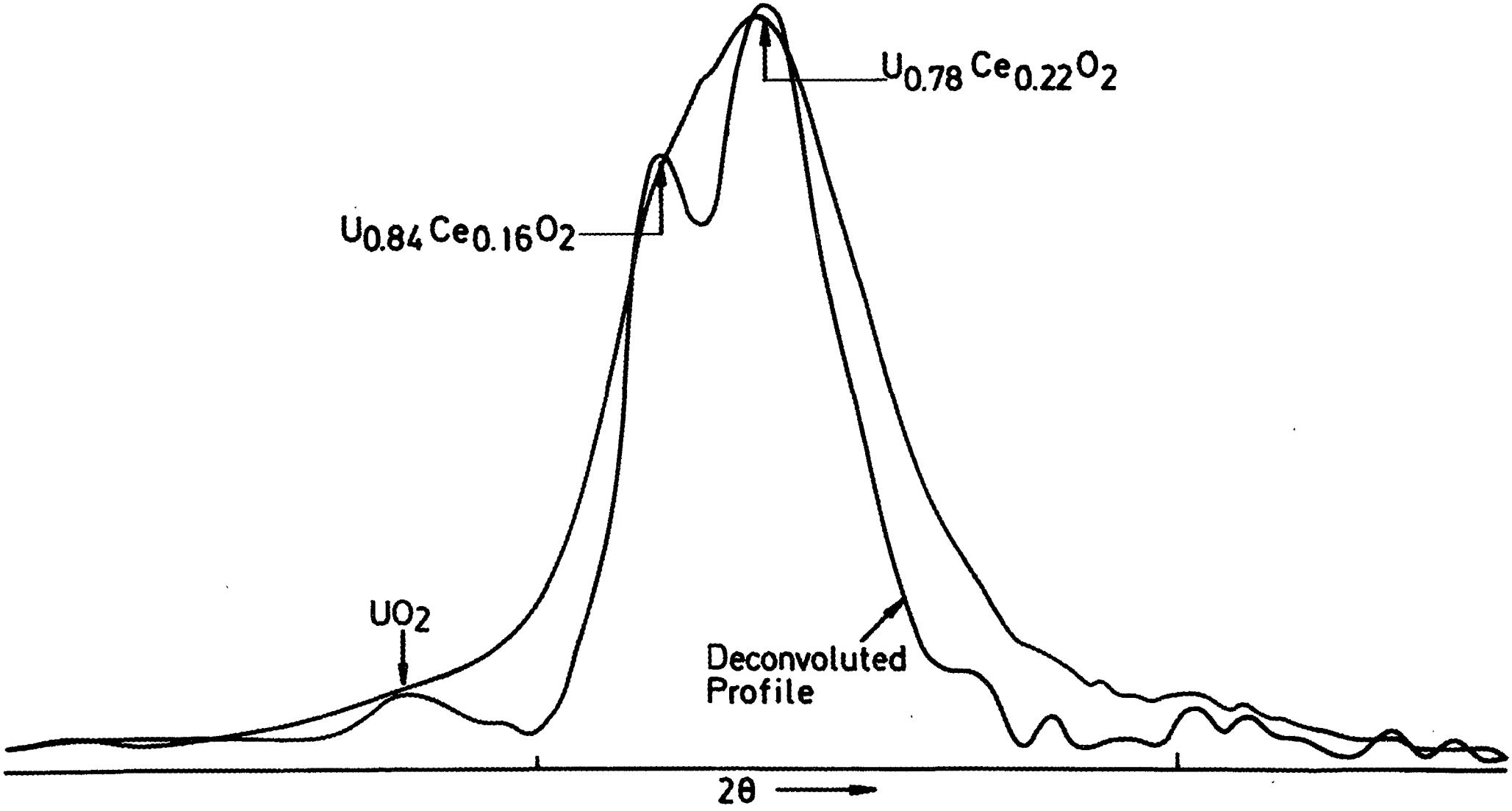

Fig.5 $K\alpha_1$ Profile of UO_2 - 20 CeO_2 before and after Deconvolution

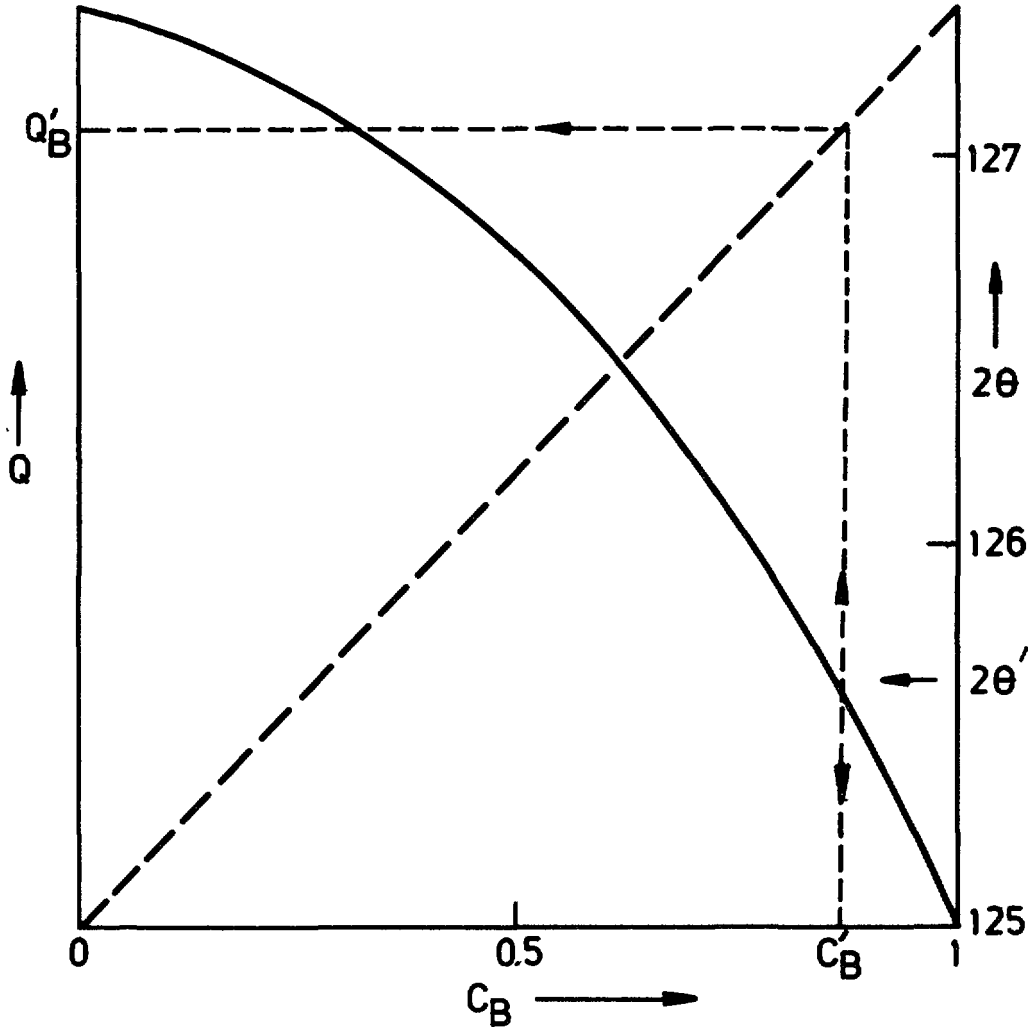

Fig.6 Diagrammatic representation of method for determining correction factor Q and concentration factor c from given values of 2θ

– – – – – Correction curve Q v C_B

——— Concentration curve C_B v 2θ

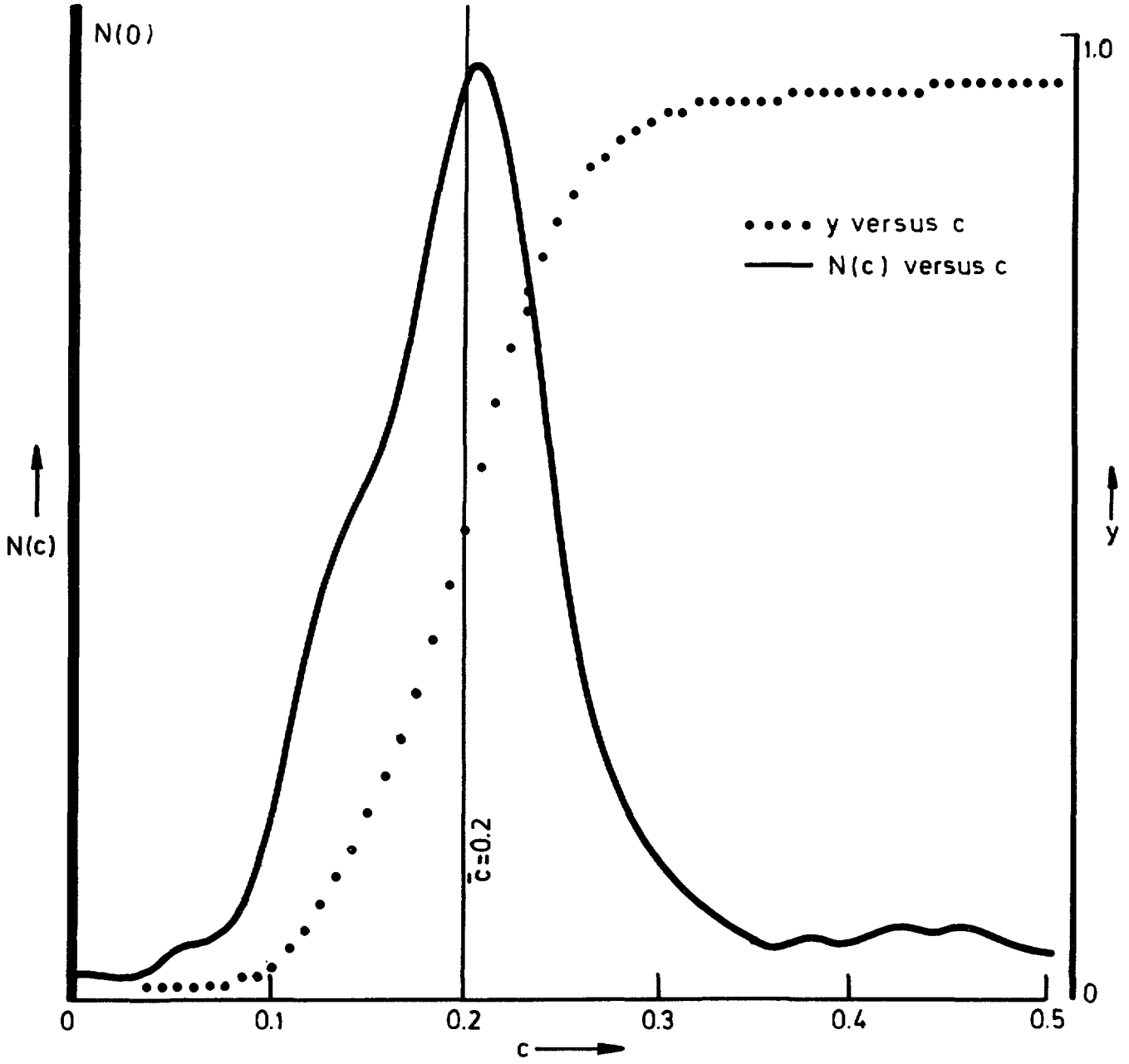

Fig.7 Frequency Distribution Curve for CeO_2 in UO_2 - 20 CeO_2

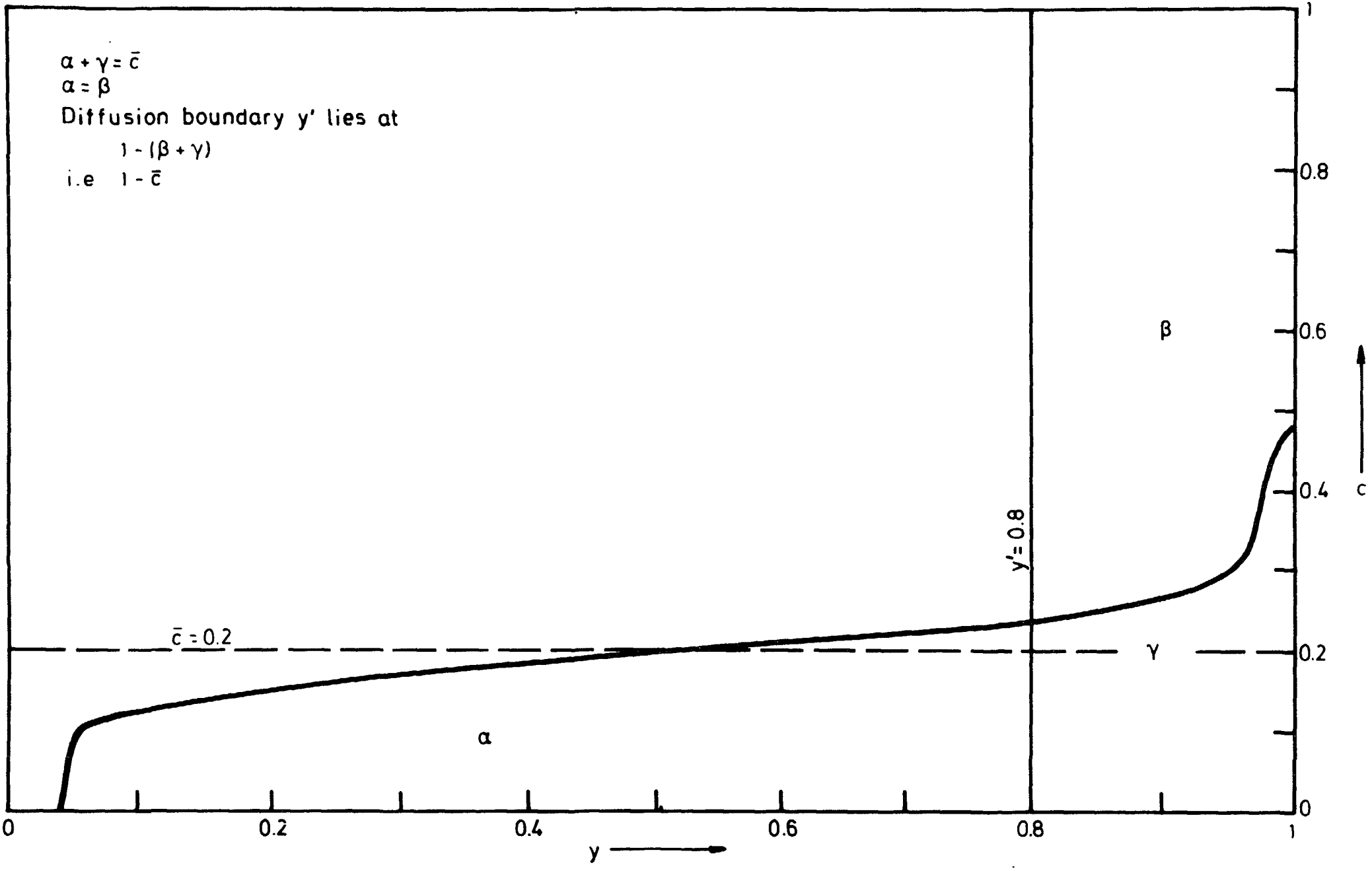

AE:s kontorstryckeri
Nyköping 1975

Fig.8 Effective Penetration Curve for UO_2 -20 CeO_2 after 32 h at 1700°C

LIST OF PUBLISHED AE-REPORTS

1—440 (See back cover earlier reports.)

441. Neutron capture gamma ray cross sections for Ta, Ag, In and Au between 30 and 175 keV. By J. Hellström and S. Beshai. 1971. 30 p. Sw. cr. 15:—.
442. Thermodynamical properties of the solidified rare gases. By I. Ebbsjö. 1971. 46 p. Sw. cr. 15:—.
443. Fast neutron radiative capture cross sections for some important standards from 30 keV to 1.5 MeV. By J. Hellström. 1971. 22 p. Sw cr. 15:—.
444. A Ge (Li) bore hole probe for in situ gamma ray spectrometry. By A. Lauber and O. Landström. 1971. 26 p. Sw. cr. 15:—.
445. Neutron inelastic scattering study of liquid argon. By K. Sköld, J. M. Rowe, G. Ostrowski and P. D. Randolph. 1972. 62 p. Sw. cr. 15:—.
446. Personnel dosimetry at Studsvik during 1970. By L. Hedlin and C.-O. Widell. 1972. 8 p. Sw. cr. 15:—.
447. On the action of a rotating magnetic field on a conducting liquid. By E. Dahlberg. 1972. 60 p. Sw. cr. 15:—.
448. Low grade heat from thermal electricity production. Quantity, worth and possible utilisation in Sweden. By J. Christensen. 1972. 102 p. Sw. cr. 15:—.
449. Personnel dosimetry at Studsvik during 1971. By L. Hedlin and C.-O. Widell. 1972. 8 p. Sw. cr. 15:—.
450. Deposition of aerosol particles in electrically charged membrane filters. By L. Ström. 1972. 60 p. Sw. cr. 15:—.
451. Depth distribution studies of carbon in steel surfaces by means of charged particle activation analysis with an account of heat and diffusion effects in the sample. By D. Brune, J. Lorenzen and E. Witalis. 1972. 46 p. Sw.cr. 15:—.
452. Fast neutron elastic scattering experiments. By M. Salama. 1972. 98 p. Sw. cr. 15:—.
453. Progress report 1971. Nuclear chemistry. 1972. 21 p. Sw. cr. 15:—.
454. Measurement of bone mineral content using radiation sources. An annotated bibliography. By P. Schmeling. 1972. 64 p. Sw. cr. 15:—.
454. Measurement of bone mineral content using radiation sources. An annotated bibliography. Suppl. 1. By P. Schmeling. 1974. 26 p. Sw. cr. 20:—.
455. Long-term test of self-powered detectors in HBWR. By M. Brakas, O. Strindehag and B. Söderlund. 24 p. 1972. Sw. cr. 15:—.
456. Measurement of the effective delayed neutron fraction in three different FR0-cores. By L. Moberg and J. Kockum. 1972. Sw. cr. 15:—.
457. Applications of magnetohydrodynamics in the metal industry. By T. Robinson, J. Braun and S. Linder. 1972. 42 p. Sw cr. 15:—.
458. Accuracy and precision studies of a radiochemical multielement method for activation analysis in the field of life sciences. By K. Samsahl. 1972. 20 p. Sw. cr. 15:—.
459. Temperature increments from deposits on heat transfer surfaces: the thermal resistivity and thermal conductivity of deposits of magnetite, calcium hydroxy apatite, humus and copper oxides. By T. Kelén and J. Arvesen. 1972. 68 p. Sw. cr. 15:—.
460. Ionization of a high-pressure gas flow in a longitudinal discharge. By S. Palmgren. 1972. 20 p. Sw. cr. 15:—.
461. The caustic stress corrosion cracking of alloyed steels — an electrochemical study. By L. Dahl, T. Dahlgren and N. Lagmyr. 1972. 43 p. Sw. cr 15:—.
462. Electrodeposition of "point" $Cu^{125}I$ roentgen sources. By P. Beronius, B. Johansson and R. Söremark. 1972. 12 p. Sw. cr. 15:—.
463. A twin large-area proportional flow counter for the assay of plutonium in human lungs. By R. C. Sharma, I. Nilsson and L. Lindgren. 1972. 50 p. Sw. cr. 15:—.
464. Measurements and analysis of gamma heating in the R2 core. By R. Carlsson and L. G. Larsson. 1972. 34 p. Sw. cr. 15:—.
465. Determination of oxygen in zircaloy surfaces by means of charged particle activation analysis. By J. Lorenzen and D. Brune. 1972. 18 p. Sw. cr. 15:—.
466. Neutron activation of liquid samples at low temperature in reactors with reference to nuclear chemistry. By D. Brune. 1972. 8 p. Sw. cr. 15:—.
467. Irradiation facilities for coated particle fuel testing in the Studsvik R2 reactor. By S. Sandklef. 1973. 28 p. Sw. cr. 20:—.
468. Neutron absorber techniques developed in the Studsvik R2 reactor. By R. Bodh and S. Sandklef. 1973. 26 p. Sw cr. 20:—.
469. A radiochemical machine for the analysis of Cd, Cr, Cu, Mo and Zn. By K. Samsahl, P. O. Wester, G. Blomqvist. 1973. 13 p. Sw. cr. 20:—.
470. Proton pulse radiolysis. By H. C. Christensen, G. Nilsson. T. Reitberger and K.-Å. Thuomas. 1973. 26 p. Sw. cr. 20:—.
471. Progress report 1972. Nuclear chemistry. 1973. 28 p. Sw. cr. 20:—.
472. An automatic sampling station for fission gas analysis. By S. Sandklef and P. Svensson. 1973. 52 p. Sw. cr. 20:—.
473. Selective step scanning: a simple means of automating the Philips diffractometer for studies of line profiles and residual stress. By A. Brown and S. Å. Lindh. 1973. 38 p. Sw. cr. 20:—.
474. Radiation damage in CaF_2 and BaF_2 investigated by the channeling technique. By R. Hellborg and G. Skog. 1973. 38 p. Sw. cr. 20:—.
475. A survey of applied instrument systems for use with light water reactor-containments. By H. Tuxen-Meyer. 1973. 20 p. Sw. cr. 20:—.
476. Excitation functions for charged particle induced reactions in light elements at low projectile energies. By J. Lorenzen and D. Brune. 1973. 154 p. Sw. cr. 20:—.
477. Studies of redox equilibria at elevated temperatures 3. Oxide/oxide and oxide/metal couples of iron, nickel, copper, silver, mercury and antimony in aqueous systems up to 100°C. By Karin Johansson, Kerstin Johnsson and Derek Lewis. 1973. 42 p. Sw. cr. 20:—.
478. Irradiation facilities for LWR fuel testing in the Studsvik R2 reactor. By S. Sandklef and H. Tomani. 1973. 30 p. Sw. cr. 20:—.
479. Systematics in the (p,xn) and (p,pxn) reaction cross sections. By L. Jéki. 1973. 14 p. Sw. cr. 20:—.
480. Axial and transverse momentum balance in subchannel analysis. By S. Z. Rouhani. 1973. 58 p. Sw. cr. 20:—.
481. Neutron inelastic scattering cross sections in the energy range 2 to 4.5 MeV. Measurements and calculations. By M. A. Etemad. 1973. 62 p. Sw. cr. 20:—.
482. Neutron elastic scattering measurements at 7.0 MeV. By M. A. Etemad. 1973. 28 p. Sw. cr. 20:—.
483. Zooplankton in Tvären 1961—1963. By E. Almquist. 1973. 50 p. Sw. cr. 20:—.
484. Neutron radiography at the Studsvik R2-0 reactor. By I. Gustafsson and E. Sokolowski. 1974. 54 p. Sw. cr. 20:—.
485. Optical model calculations of fast neutron elastic scattering cross sections for some reactor materials. By M. A. Etemad. 1974. 165 p. Sw. cr. 20:—.
486. High cycle fatigue crack growth of two zirconium alloys. By V. S. Rao. 1974. 30 p. Sw. cr. 20:—.
487. Studies of turbulent flow parallel to a rod bundle of triangular array. By B. Kjellström. 1974. 190 p. Sw. cr. 20:—.
488. A critical analysis of the ring expansion test on zircaloy cladding tubes. By K. Pettersson. 1974. 8 p. Sw. cr. 20:—.
489. Bone mineral determinations. Proceedings of the symposium on bone mineral determinations held in Stockholm-Studsvik, Sweden, 27-29 may 1974.
    Vol. 1. Presented papers. 1974. 170 p. Sw. cr. 20:—.
    Vol. 2. Presented papers (cont.) and group discussions. 1974. 200 p. Sw. cr. 20:—.
    Vol. 3. Bibliography on bone morphometry and densitometry in man. By A. Horsman and M. Simpson. 1974. 112 p. Sw. cr. 20:—.
490. The over-power ramp fuel failure phenomenon and its burn-up dependence — need of systematic, relevant and accurate irradiation investigations. — Program proposal. By H. Mogard. 1974. Sw. cr. 20:—.
491. Phonon anharmonicity of germanium in the temperature range 80—880 K. By G. Nelin and G. Nilsson. 1974. 28 p. Sw. cr. 20:—.
492. Harmonic lattice dynamics of germanium. By G. Nelin. 1974. 32 p. Sw. cr. 20:—.
493. Diffusion of hydrogen in the β-phase of Pd-H studied by small energy transfer neutron scattering. By G. Nelin and K. Sköld. 1974. 28 p. Sw. cr. 20:—.
494. High temperature thermocouple applications in the R2-reactor, Studsvik. By B. Rohne. 1974. 20 p. Sw. cr. 20:—.
495. Estimation of the rate of sensitization in nickel base alloys. By J. Wiberg. 1974. 14 p. Sw. cr. 20:—.
496. A hort-el-complex in Sweden. By J. Christensen. 1974. 82 p. Sw. cr. 20:—.
497. Effect of wall friction and vortex generation on radial void distribution — the wall-vortex effect. By Z. Rouhani. 1974. 36 p. Sw. cr. 20:—.
498. The deposition kinetics of calcium hydroxy apatite on heat transfer surfaces at boiling. By T. Kelén and R. Gustafsson. 1974. 30 p. Sw. cr. 20:—.
499. Observations of phases and volume changes during precipitation of hydride in zirconium alloys. By G. Östberg, H. Bergqvist, K. Pettersson, R. Attermo, K. Norrgård, L-G. Jansson and K. Malén. 1974. 16 p. Sw. cr. 20:—.
500. X-ray elastic constants for cubic materials. By K. Malén. 1974. 25 p. Sw. cr. 20:—.
501. Electromagnetic screening and skin-current distribution with magnetic and non-magnetic conductors. By E. Dahlberg. 1974. 44 p. Sw. cr. 20:—.
502. Depth distribution studies of carbon, oxygen and nitrogen in metal surfaces by means of neutron spectrometry. By. J. Lorenzen. 1975. 54 p. Sw. cr. 20:—.
503. A systematic study of neutron inelastic scattering in the energy range 2.0 to 4.5 MeV. By E. Almén-Ramström. 1975. 108 p. Sw. cr. 20:—.
504. Analysis of EPR with large quadrupole interaction. By K.-Å. Thuomas. 1975. 28 p. Sw. cr. 20:—.
505. Observations on deformation systems in zircaloy-2 deformed at room temperature. By K. Pettersson and H. Bergqvist. 1975. 20 p. Sw. cr. 20:—.
506. Study of a tritium-fueled battery utilizing the difference of workfunction between electrodes. By J. Braun. 1975. 20 p. Sw. cr. 20.—.
507. X-ray Characterization of non-equilibrium solid solutions. By A. Brown and Ö. Rosdahl. 1975. 30 p. Sw. cr. 20:—.

List of published AES-reports (In Swedish)

1. Analysis by means of gamma spectrometry. By D. Brune. 1961. 10 p. Sw. cr. 6:—.
2. Irradiation changes and neutron atmosphere in reactor pressure vessels-some points of view. By M. Grounes. 1962. 33 p. Sw. cr. 6:—.
3. Study of the elongation limit in mild steel. By G. Östberg and R. Attermo. 1963. 17 p. Sw. cr. 6:—.
4. Technical purchasing in the reactor field. By Erik Jonson. 1963. 64 p. Sw. cr. 8:—.
5. Ägesta nuclear power station. Summary of technical data, descriptions, etc. for the reactor. By B. Lilliehöök. 1964. 336 p. Sw. cr. 15:—.
6. Atom Day 1965. Summary of lectures and discussions. By S. Sandström. 1966. 321 p. Sw. cr. 15:—.
7. Building materials containing radium considered from the radiation protection point of view. By Stig O. W. Bergström and Tor Wahlberg. 1967. 26 p. Sw. cr. 10:—.
8. Uranium market. 1971. 30 p. Sw. cr. 15:—.
9. Radiography day at Studsvik. Tuesday 27 april 1971. Arranged by AB Atomenergy, IVA's Committee for nondestructive testing and TRC AB. 1971. 102 p. Sw. cr. 15:—.
10. The supply of enriched uranium. By M. Mårtensson. 1972. 53 p. Sw. cr. 15:—.
11. Fire studies of plastic-insulated electric cables, sealing lead-in wires and switch gear cubicles and floors. 1973. 117 p. Sw. cr. 35:—.
12. Soviet–Swedish symposium on reactor safety problems. Studsvik, march 5–7, 1973.
    Part 1. Swedish papers. 1973. 109 p. Sw. cr. 20:—
    Part 2. Soviet papers. 1973. 120 p. Sw. cr. 20:—.
13. International and national organizations within the nuclear energy field. By S. Sandström. 1975. 24 p. Sw. cr. 20:—.
14. Energy analysis and power growth patterns. By K. Jirlow. 1975. 44 p. Sw. cr. 20.—.

Additional copies available from the Library of AB Atomenergi, Fack, S-611 01 Nyköping 1, Sweden.

Pogo Print, Stockholm 1975